Neural integration underlying a time-compensated sun compass in the migratory monarch butterfly

Supplementary Material

Eli Shlizerman[1], James Phillips-Portillo[2], Daniel B. Forger[3*], Steven M. Reppert[2]

1 Department of Applied Mathematics, Department of Electrical Engineering, University of Washington, Seattle, WA, 98195, USA
2 Department of Neurobiology, University of Massachusetts Medical School, Worcester, MA, 01605, USA
3 Department of Mathematics, Department of Computational Medicine and Bioinformatics, University of Michigan, Ann Arbor, MI, 48104, USA
* Corresponding Author

1. Computational Methods (Supplement for Fig. 2)

1.1. Lyapunov Function

The requirement for a line attractor in the system defined in Eq. (1) can be formulated as two conditions on squared difference between the inputs, defined by the function $V(A;T)$, where A is considered as a variable and T as a parameter

$$V(A;T) = (\varphi(I_l) - \varphi(I_r))^2. \quad (5)$$

This function resembles a potential, such that any point on the potential (particular choice of A and T) will evolve to the minimum point. The function is nonnegative and thus has a minimum at 0, when $I_l = I_r$. Showing that the balanced state A_{fp} is a unique fixed point, in the interval $A \in (135,315)$ for each $T \in [0,12]$, is equivalent to showing that the function V vanishes on $A = A_{fp}$ and positive for $A \neq A_{fp}$:

$$V(A;T)|_{A=A_{fp}} = 0 \quad \text{and} \quad V(A;T)|_{A\neq A_{fp}} > 0. \quad (6)$$

For other values of A we require that the inputs will drive the firing-rates f_l and f_r towards the balanced state such that A will be attracted back to the fixed point A_{fp}. This requirement can be formulated as a condition on the function $V(A;T)$ as well. We require that the time derivative of $V(A;T)$ will be negative and by using the chain rule and Eq. (2) derive the following condition

$$\frac{dV(A;T)}{dt} = \frac{\partial V}{\partial A}\frac{dA}{dt} = \frac{\partial V}{\partial A}(f_l - f_r) < 0, \quad \text{for } A \neq A_{fp}. \tag{7}$$

The condition involves variables f_l, f_r and A. To simplify it, we assume that the dynamics inf_l, f_r are fast enough such that f_l rapidly follows $\varphi(I_l)$, f_r rapidly follows $\varphi(I_r)$. We can then replace the term $(f_l - f_r)$ in Eq. (7) by $(\varphi(I_l) - \varphi(I_r))$ and derive the following condition

$$\frac{\partial V}{\partial A}((\varphi(I_l) - \varphi(I_r)) < 0, \quad \text{for } A \neq A_{fp}. \tag{8}$$

Due to our assumption on the dynamics of f_l and f_r the condition is necessary for convergence to the balanced state A_{fp}, but not sufficient. Indeed it is possible to set our initial conditions such that the trajectory does not converge to the balanced state and will be crossing the unstable fixed point. These phenomena are part of the dynamics of the simulated compass and we discuss them in the Results section. However we can always guarantee that for small enough initial velocity the balanced state will be attainable and condition (6) in conjunction with (8) will then be sufficient for A_{fp} to be a line attractor.

1.2. Verification of stability for the proposed integration mechanism

For signals $NS1, NS2, NCLK1, NCLK2$ depicted in **Fig. 1.** , we check that the integrating functions I_l and I_r that we choose in Eq. (4) satisfy conditions (6) and (8) for the stability of the balanced state. The signals are defined as

$$NS1 = \frac{I_b}{2}\left(1 - \sin\frac{a\pi}{180}\right), \qquad NS2 = \frac{I_b}{2}\left(1 + \cos\frac{a\pi}{180}\right),$$
$$NCLK1 = \frac{I_b}{2}\left(1 - \cos\frac{\pi(\tau+3)}{12}\right), \qquad NCLK2 = \frac{I_b}{2}\left(1 - \sin\frac{\pi(\tau+3)}{12}\right), \quad (9)$$

where I_b is the base firing-rate, $a \in mod([-180,180], 360)$ is the azimuthal angle and $\tau \in [-12,12]$ is ZT with $ZT = 0$ representing the sunrise and $\mathrm{ZT} = 12, -12$ representing the sunset.

Verification of Condition (6): The functions I_l and I_r are antisymmetric, such that $I_l = -I_r$. This property assures that $V(A;T) = 0$, only when both $I_l = 0$ and $I_r = 0$. This occurs only when $D_1 = -D_2$. The solution of this equation is unique and equal to $A = A_{fp}$ as required and illustrated in **Fig. 2** as the black line at $V(A,T) = 0$.

Verification of Condition (8): We compute the derivative $\partial V/\partial A$

$$\frac{\partial V}{\partial A} = 2(\varphi(I_l) - \varphi(I_r))(\partial\varphi(I_l)/\partial A - \partial\varphi(I_r)/\partial A), \quad (10)$$

where $\varphi(I_l)$ and $\varphi(I_r)$ are piecewise continuous functions and their derivatives taken piecewise as well. We multiply the derivative by the term $(\varphi(I_l) - \varphi(I_r))$, as in Condition (8), such that the inequality becomes

$$2(\varphi(I_l) - \varphi(I_r))^2(\partial\varphi(I_l)/\partial A - \partial\varphi(I_r)/\partial A) < 0, \quad (11)$$

which has to be satisfied for stability. Since the first term is positive we analyze the sign of the second term. In the interval A: $(135,315)$, for any T, the function $I_l(A)$ is monotonically decreasing function and $I_r(A)$ is monotonically increasing (as shown in **Fig. S 2. A).** Thereby the sign of the second term in Eq. (11) is always negative and thereby the stability condition (8) is satisfied.

Separatrix: The instability of the fixed point $A_{ufp}(T) = mod(135 + 15T\,, 360)$ for $T \in [0,12]$ is established by flipping the signs of the inequality in Condition (8) such

that trajectories will be repelled from the fixed point. Indeed, in the complementary interval A: $(315\ ,135)$ the input functions $I_l(A)$ and $I_r(A)$ flip direction and become monotonically increasing and decreasing, respectively, such that the derivative term is positive.

1.3. Other configurations

To test the uniqueness of the proposed neural circuit for SW migration, we explore whether there are additional wirings that permit a stable flight direction during the day. There are $2^8 = 256$ candidate circuits to examine, since there is a total of 8 input signals into the neural circuit (4 into left unit and 4 into right unit) and we allow each input wiring to be excitatory (+) or inhibitory (-).

Our analysis shows that there is *only one circuit* capable to direct the flight to a stable direction, the southwest, at all times of day, and it is the circuit defined in Eq. (4 **).**

To narrow down the number of circuit configurations we note that for the condition in Eq. (6) to be satisfied, i.e., ensure existence of fixed points, the functions I_l and I_r are required to be antisymmetric, such that $I_l = -I_r$, which corresponds to axisymmetric anatomy of the monarch. Therefore we consider the possible wirings for I_l

$$I_l = \pm NCLK1 \pm NCLK2 \pm NS1 \pm NS2$$

and I_r is set as $-I_l$. There are four connections that determine I_l, each of which can be $+$ or $-$, incorporating 16 combinations. Out of these combinations, only those with two $+$ and two $-$ connections will support fixed points for all times of day, which leaves us with $\binom{4}{2} = 6$ combinations summarized in Table S 1.

Comb #	NCLK1	NCLK2	NS1	NS2
1	+	+	−	−
2	−	−	+	+
3	+	−	+	−
4	−	+	−	+
5	+	−	−	+
6	−	+	+	−

Table S 1: Circuit configurations that can potentially support stable flight direction.

Combination #1 is the circuit described in Eq. (4). To analyze other combinations we note that there is additional symmetry, which corresponds to pairs of combinations (rows #1-2,#3-4,#5-6), where in each pair the combinations are antisymmetric to each other (e.g. $\#3 = -\#4$).The symmetry determines that the fixed points in both combinations in each pair are positioned at the same angular position and rotation directions are being flipped (correspondingly stability is flipped). We therefore conclude that combination #2 will have same position of the fixed points as in #1. However, stability is flipped such that the southwest direction is unstable and the second fixed point, which rotates during the day, is stable. Therefore combination #2 does not support any stable flight directions for the duration of the day.

For combinations #3-4 there are two fixed points, as shown in **Fig. S 2.** At T=0, combination #3 fixed points are positioned at the southwest and the northeast direction. The fixed point at the southwest direction remains fixed during the day while the second fixed point makes full rotation. Stability analysis indicates that the fixed points switch their stability in the middle of the day (T=6). In particular, the southwestern fixed point is initially stable while the rotating fixed point is unstable. In the middle of the day, at T=6, the fixed points merge and southwest fixed point looses its stability to the rotating fixed point. For combination #4 fixed points positioned at same directions and switch in

stability occurs: southwestern fixed point begins with being unstable and switches to being stable at T=6. We thus conclude that combinations #3-4 do not support a stable fixed flight direction during the whole day.

Combinations #5-6 also do not support stable flight directions. Here the northeastern fixed point is fixed while the fixed point that is initially positioned at the southwest rotates. Stability analysis indicates that these fixed points switch their stability as in the case of combinations #3-4.

1.4. Solar Azimuth Receptive Fields

Neural encoding of solar azimuth position is modeled as a series of neurons with visual receptive fields that carry information from the compound eye to the CX, innervating the LAL. The neural cascade that detects the sun's relative azimuth is initiated by the brightest point in the field of view, activating photoreceptor cells in a subset of ommatidia of one eye. Here we treat the sun as a point source so that the intensity of activation for photoreceptors in a given ommatidia is determined by its location on the spherical surface of the eye. In particular, cells that respond with the highest intensity have their photoreceptor terminals in the ommatidia aligned with the sun's direction. Spreading to neighboring ommatidia, the intensity of activation decays according to Lambert's law, which dictates that the intensity is proportional to the dot product of surface normals and light direction (Pedrotti et al. 1993). By approximating the eyes of the monarch as two hemispheres, separated by 180 degrees pointing outwards, we establish that a simple mechanism for detection of the solar azimuth is integration of the luminance captured by all ommatidia in each eye. For example, for the left eye, the luminance from a rotating light source is maximally captured when the light is positioned directly to the left. When the light rotates from that position, the luminance gradually decays, reaching a minimum when the light is on the right side (**Fig. 1.** B). For the right eye, the scenario is reversed: the right position produces the greatest captured luminance and almost no light is captured when the light is positioned on the left.

1.5. Integration Model and Simulations Parameters

Sensory azimuth and time encoding signals (expressed by computational neurons) are the following functions

$$\begin{aligned} NS1(A) &= \frac{I_b}{2}\left(1-\sin\frac{A\pi}{180}\right), & NS2(A) &= \frac{I_b}{2}\left(1+\cos\frac{A\pi}{180}\right), \\ NCLK1(T) &= \frac{I_b}{2}\left(1-\cos\frac{\pi(T+3)}{12}\right), & NCLK2(T) &= \frac{I_b}{2}\left(1-\sin\frac{\pi(T+3)}{12}\right), \end{aligned} \quad (12)$$

where I_b is set to 40Hz. The azimuth function is determined from half sphere model of the eyes while the clock function is determined according to recordings from antennae, molecular curves and requiring these signals to match in peak and trough amplitudes. The integration model, implemented with left and right firing units, f_l and f_r , receives inputs that are a combination of the sensory signals

$$\begin{aligned} D_1 &= NCLK1(T) - NS1(A), & D_2 &= NCLK2(T) - NS2(A), \\ I_l(A,T) &= D_1 + D_2, & I_r(A,T) &= -D_1 - D_2. \end{aligned} \quad (13)$$

where I_l and I_r are inputs into left and right units respectively. The units are implemented as continuous differential equations denoting the angular velocity (deg/sec) with linear threshold inputs and rapid self-decay rate

$$\begin{aligned} \frac{df_l}{dt} &= -\alpha f_l + \beta\varphi(I_l(A,T)), \\ \frac{df_r}{dt} &= -\alpha f_r + \beta\varphi(I_r(A,T)), \end{aligned} \qquad \varphi(x) = \begin{cases} 0 & x < 0, \\ x & x \geq 0. \end{cases} \quad (14)$$

where $\alpha = 100, \beta = 3.25$. The output of firing rate units is then integrated to find the angular position x_A (deg)

$$\frac{dx_A}{dt} = \gamma(f_l - f_r). \quad (15)$$

where $\gamma = 16$. For computing convergence timescales to SW orientation, simulations are initiated with zero velocity $f_l(0) = 0, f_r(0) = 0$ in a deterministic setup. Deterministic

setup was used for producing ease-in panel dynamics (at ZT=2 with initial condition chosen close to separatrix). To simulate the dynamic environment of the monarchs and dependence on initial conditions we also incorporate noise into the system modeled by $\eta(t)$ as additive noisy input terms $I = I^{det} + \eta(t)$. To simulate persistent input noise, $\eta_p(t)$ is modeled by a Weiner stochastic process with $N(0,2)$ distribution (up to 5% variation of the input signals). We also occasionally include strong kicks, e.g., to simulate random strong perturbations by adding a term $\eta_s(t)$ drawn from $N(0,12)$ distribution every 3 sec (up to 30% variation of the input signals).

2. Experimental Supplementary Information and Methods (Supplement for Fig. 1 & Fig. 2 and Results)

2.1. Animals

Migrating monarch butterflies were captured from roosts in western Massachusetts and kept in the laboratory in Percival incubators set to provide autumn-like environmental conditions known to preserve migratory behavior: an 11 hr light period at 23°C followed by a 13 hr period of darkness at 12°C. Animals were fed a solution of 25% honey in water three times each week.

2.2. Visual Stimulus

Visual stimuli were provided through 4 LED light sources as described in Heinze and Reppert (2011). Briefly, light emitting diodes with peak emissions at 365 nm (Ultraviolet, UV), 460 nm (blue), and 520 nm (Green) each subtending a visual angle of 3° were mounted to a radial sage so that they could be rotated completely about the animals head at an elevation of 25° – 30° in both directions. For these experiments light stimuli were rotated at a rate of 60° / sec first in the anti-clockwise and then in the clockwise direction.

2.3. Intracellular recordings

Intracellular recordings were conducted during the light phase of each animals light dark cycle. For recordings, wings and legs were removed and animals were secured to a metal support for consistent positioning relative to the stimulating apparatus. The head capsule was opened frontodorsally and the perineural sheath weakened with protease before thorough rinsing with physiological saline (150 mM NaCl, 3 mM KCl, 10 mM TES, 25 mM sucrose, 3 mM CaCl2; pH = 6.9; King et al., 2000) and removal with forceps. After these preparatory steps, animals were mounted in the experimental setup and aligned so the stimulating apparatus was directly above the the head and the recording electrode could access the brain frontally. The lateral accessory lobes were chosen as the target recording site because they receive both projections from the visual neuropils and from the central complex, the collection of midline neuropils thought to serve as the substrate for sun compass integration (Heinze & Reppert 2011).

Intracellular recordings were performed with the indifferent electrode placed in the head capsule opening and sharp electrodes drawn from borosilicate glass to a tip resistance 60–150 MΩ. Electrodes were filled with 4% Neurobiotin dissolved in 1 M KCl and backfilled with 1 M KCl. Neuronal activity was amplified with an NPI SEC05-LX amplifier (NPI electronic GmbH, Tamm, Germany), digitized at a sampling rate of 5 kHz using a CED 1401 (Cambridge Electronic Design Limited, Cambridge, England) analog to digital converter and recording using CED spike 2 software. Spike times were extracted and recordings analyzed using custom scripts in Matlab (The Mathworks, Natick MA).

After recording, injection of depolarizing current (1-3 nA for 1-5 min) was used to pass neurobiotin into the subject neuron. Neurobiotin tracer was allowed to diffuse throughout the recorded neuron for approximately for 20 min while the brain was kept from desiccating with saline. After this period the brain was removed from the head capsule and fixed in 4% paraformaldehyde 0.25% glutaraldehyde and 2% saturated picric acid in 0.1 M phosphate buffer. Brains were allowed to fix over night at 4°C and were then washed in 0.1M phosphate buffered saline. To visualize the neurons from which recordings were made brains were incubated with Cy3-conjugated Streptavidin (1:1000)

for 3 days at 4°C and then dehydrated through an ethanol series, cleared in methylsalicylate, and mounted between two coverslips so that both either side would be available for confocal microscopy.

2.4. Analysis of LAL-LAL Recordings

From recordings from the LALs, neurons that responded to rotating light sources with changes in their firing frequency were selected for more thorough characterization. We recorded from and labeled five neurons that displayed an azimuth response in preparations in which no other neurons were labeled and so the morphology of these cells could conclusively be linked to their responses. All of these neurons projected from one LAL to the other (LAL-LAL) via the mediolateral antennocerebral tract and characteristically exhibited an increase in firing rate as the presented light source passed through a preferred azimuth in the visual field. However, recorded responses were found to depend on several factors beyond the preferred azimuth, and the magnitude of the response changed with the direction of rotation and the color of the light stimulus presented.

Summing or averaging these responses produces no consistent pattern. Instead, the recorded firing rate were found to depend on a combination of visual motion and stimulus color, suggesting that these neurons function as more than motion detectors with a prescribed ungula of the visual field. However, when we compared responses to one visual stimulus at several points throughout the day we found that these neurons do respond selectively to the moving light source and provide us with insight into the possible contribution that these neurons make to the time-compensated sun compass. These responses were obtained by green (520 nm) light stimulus rotated about the animals head clockwise and counterclockwise (**Fig S1)**.

The intrinsic LAL-LAL neurons that we have recorded from were found to be sensitive to the azimuthal position of the light source. The firing rate produced in response to a rotating light stimulus is non-uniform across the visual field such that particular

azimuthal angles evoke high firing rates, while other angles do not evoke a response. Further, the responses were most selective for rotation during the midday period and less selectivity at dawn and dusk. Taking into account these findings we proceeded with an examination of the recorded responses and their relevance to the integration of time and azimuth signals rather than representing a single signal.

We have ordered these responses by the Zeitgeber time (ZT) at which the recording was performed, and determined background firing rates from periods in the recordings during which no light stimulus was presented. We found that this group of neurons appears to be time sensitive. Background firing rates increase monotonically over the course of the day (B left). Similar results where obtained when comparing the firing rate observed when the light stimulus passed through 225 degrees, the position for which azimuth input is expected to be minimal (B left). These experimentally determined that firing rates are consistent with the expected summed firing-rates of NCLK1 and NCLK2 neurons in a 'no stimulus' scenario in which the input from the azimuth NS1 and NS2 neurons is blocked (B right).

Comparing recordings for clockwise and counterclockwise stimulus rotations, we found that even though the mean firing-rate is similar for all neurons, the preferred azimuth, and the light position that evokes the smallest response depends on the direction of rotation. In this respect, responses appear to be approximately opposite to each other: when the curve that corresponds to counterclockwise rotation attains its peak, the curve that corresponds to clockwise rotation attains a trough. This suggests that LAL-LAL neurons incorporate the direction of rotation in their responses in addition to circadian clock and solar azimuth signals. This observation is consistent with recent experiments on the neural mechanisms that underlie figure tracking in flies (Bahl et al. 2013). Given these observations, we hypothesize that the neurons we have recorded from are involved in driving motor output and indicate a needed rotation direction for course correction. In particular, their activity appears to be correlated with rotation such that the direction of a necessary correction, the quantity F, can be read from their firing rates. To

test this hypothesis, we consider the difference between the clockwise and counterclockwise firing-rate curves, with the assumption that clockwise curve corresponds to f_l dynamics and counterclockwise corresponds to the f_r dynamics (C).

To analyze the difference curves obtained, we mark by vertical bars the angles corresponding to the fixed points that our model predicts (red for stable and cyan for unstable). We also highlight with a red opaque background color the unidirectional interval, between the unstable and stable fixed points, in which the butterfly is expected to correct its flight in the left direction (clockwise direction for rotating light stimulus). With these guidelines, we observe that the curve has several similarities with the expected curve for the angle correction F. First, fixed points are located in proximity to zero values of the signal. For 4 out of 5 recordings, and very close in the 5th recording, the difference curve attains a maximum in the highlighted interval and a minimum in the complementing interval. Indeed F, when rotating the light source, is expected to achieve such extremum values in these intervals. In addition, we observe sharp slopes in the curve near the predicted fixed points. Our model predicts slopes as well, since when a fixed point is being crossed, a sharp slope in F designates a switch in direction.

2.5. Electroantennograms

Electroantennograms (EAGs) were recorded as the potential difference between the tip of the antenna and the head capsule using the same amplification and recording equipment as our intracellular recordings. For these recordings both electrodes were chlorates silver wires. The indifferent electrode was again placed in the head capsule, inserted through a pin-prick affording the smallest hole possible. The animal was again fixed in place using wax and the the antenna held with tape to maintain contact with the recording electrode. Connectivity between the recording electrode and the antenna was assured through the use of electro conductive gel typically used for electrocardiograms. EAG signals were sampled for 10 min ever hour for the duration of the recording period and analyzed using fast Fourier transform to determine the relative power at all frequencies above 65 Hz.

References

Bahl, A. et al., 2013. Object tracking in motion-blind flies. *Nature neuroscience*, 16(6), pp.730–738.

Heinze, S. & Reppert, S.M., 2011. Sun compass integration of skylight cues in migratory monarch butterflies. *Neuron*, 69(2), pp.345–358.

Merlin, C., Gegear, R.J. & Reppert, S.M., 2009. Antennal circadian clocks coordinate sun compass orientation in migratory monarch butterflies. *Science*, 325(5948), pp.1700–1704.

Pedrotti, F. L., Pedrotti, L. S., & Pedrotti, L. M. (1993). *Introduction to optics* (Vol. 2). Prentice-Hall Englewood Cliffs.

3. Supplementary Figures

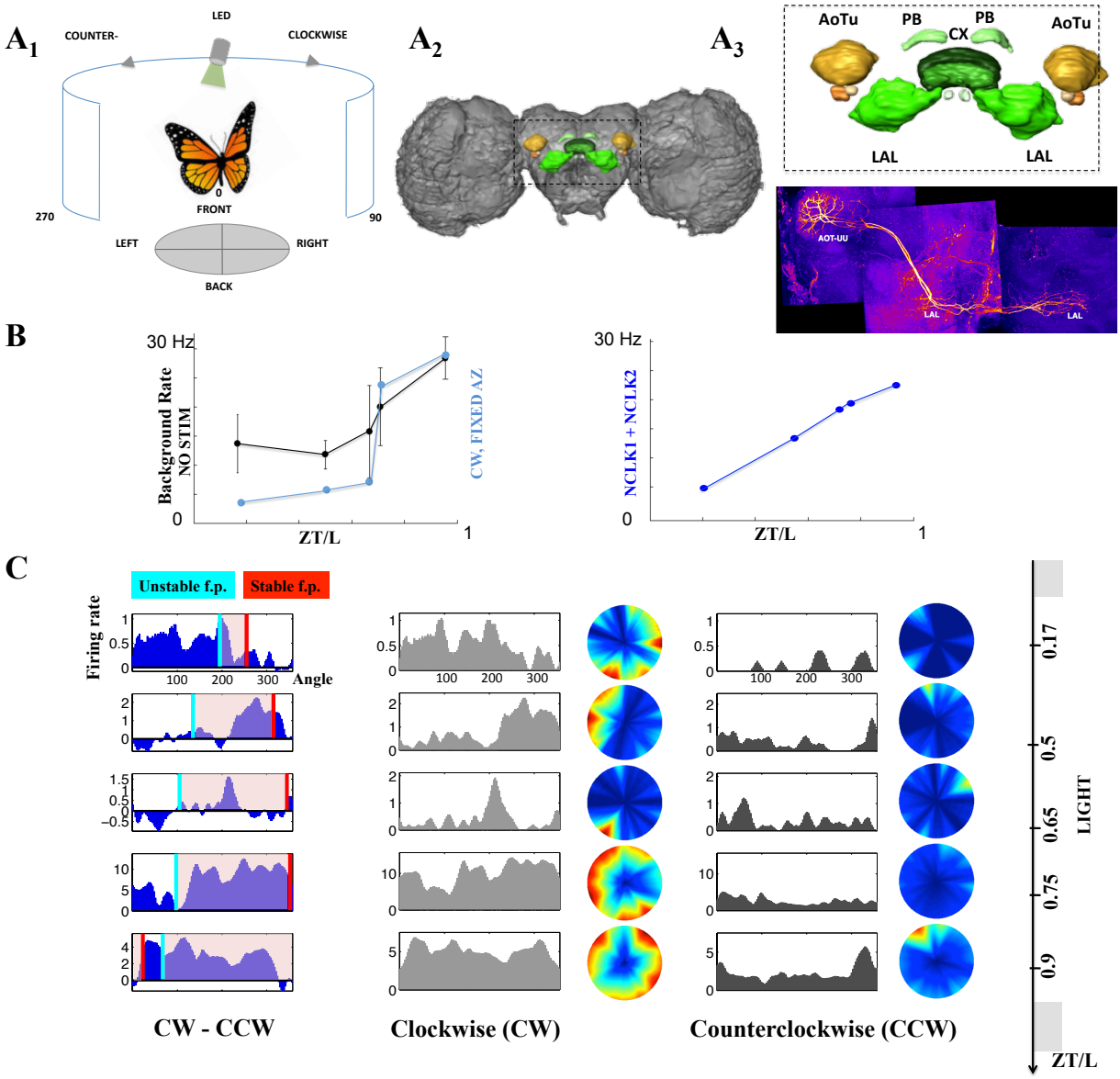

Fig. S 1. A_1 (Supplement for Fig. 2): Experimental setup to record from LAL intrinsic presumably sun-compass integrating neurons. Light source of green color is rotated with the angular velocity of 60 deg/sec while the butterfly is fixed in front position. During light rotation intracellular neuronal activity is recorded. **A_2:** 3D visualization of the Monarch brain with neuropils related to sun compass integration are being highlighted. **A_3** top: central brain neuropils thought to be involved in sun compass integration. **A_3** bottom: putative neural

pathway involved in azimuth processing: neurons connecting the AoTu to the LALs followed by neurons interconnecting the two LALs. **B:** The background firing-rate of LAL-LAL neurons (in the absence of any applied stimulus) increases over the course of the day (Left, black: recorded, no stim ($P < 0.01$), Left, cyan: recorded CW at angle of 225 degrees, Right: model). **C:** Left: Difference between clockwise (CW) and counterclockwise(CCW) firing rate curves (peristimulus time histograms, computed for moving window of 3 deg (50 msec)) of intrinsic LAL neurons (5 different neurons) recorded at different times of day: while the light stimulus is rotated (60 deg/sec rotation speed). The difference designates the curve. Estimated fixed points locations computed by the model are represented as bars - cyan - unstable and red -stable. Unidirectional correction interval for CW rotation (left) is highlighted with red opaque color. Middle: CW rotation, Right: CCW rotation. Firing rate curves are also represented as color maps, high values are identified with red color and low values with blue color

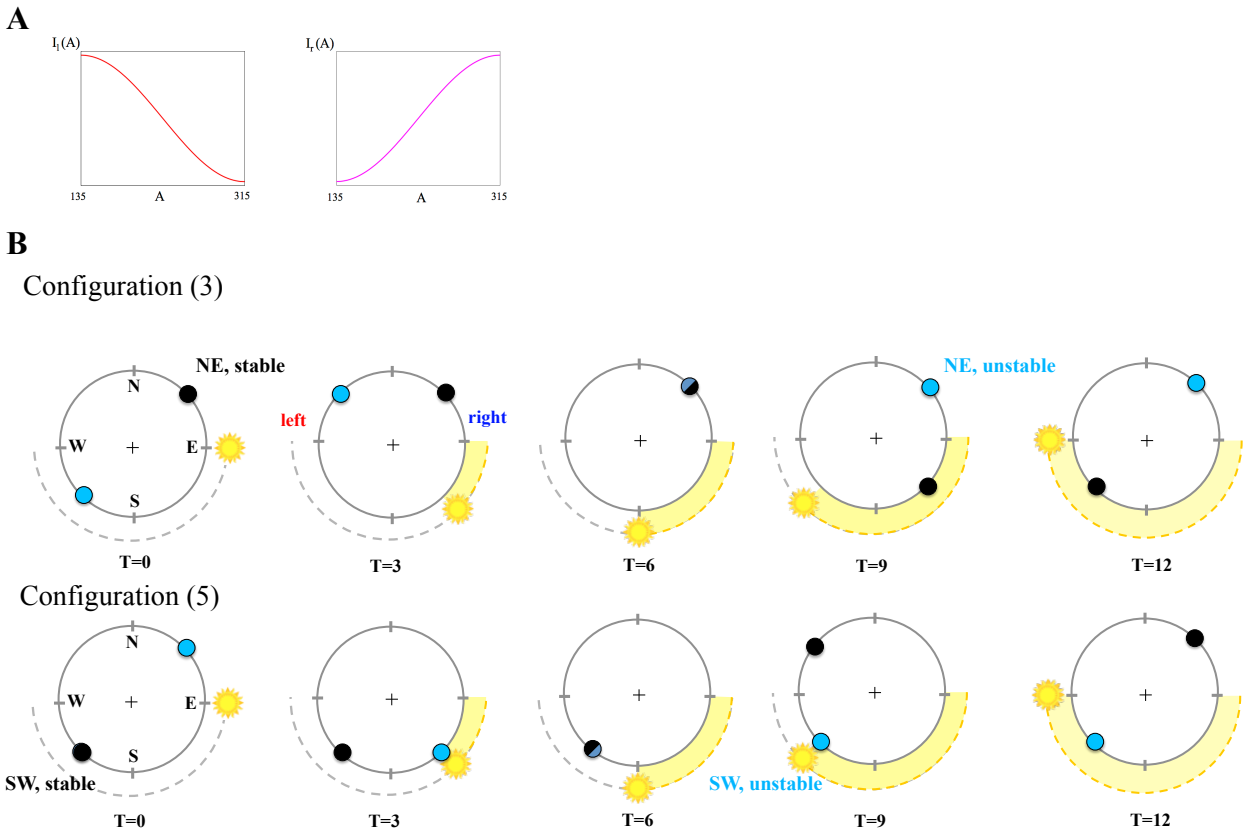

Fig. S 2. A (supplement for Fig. 2) The functions $\mathbf{I_l}$ $(\mathbf{A})$ and $\mathbf{I_r}(\mathbf{A})$ in the interval $\mathbf{A} = (\mathbf{135°}, \mathbf{315°})$. B: Angular positions of fixed points at different times for (unstable) configurations (3 top and 5 bottom). Top: Balanced fixed point is positioned at the NE and looses stability at T=6 to the rotating fixed point. Bottom: Balanced fixed point is positioned at the SW and looses stability at T=6 to the rotating fixed point.

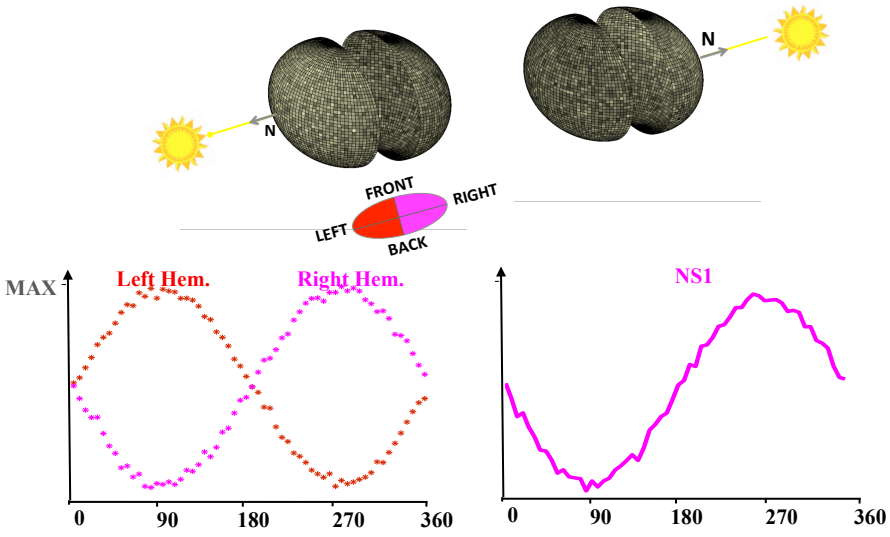

Fig. S 3. (supplement for Fig. 1) Repetition of receptive fields setup as in **Fig. 1.** B, with noisy (white noise) reception of the luminance and elevation of the light source of 40 degrees.

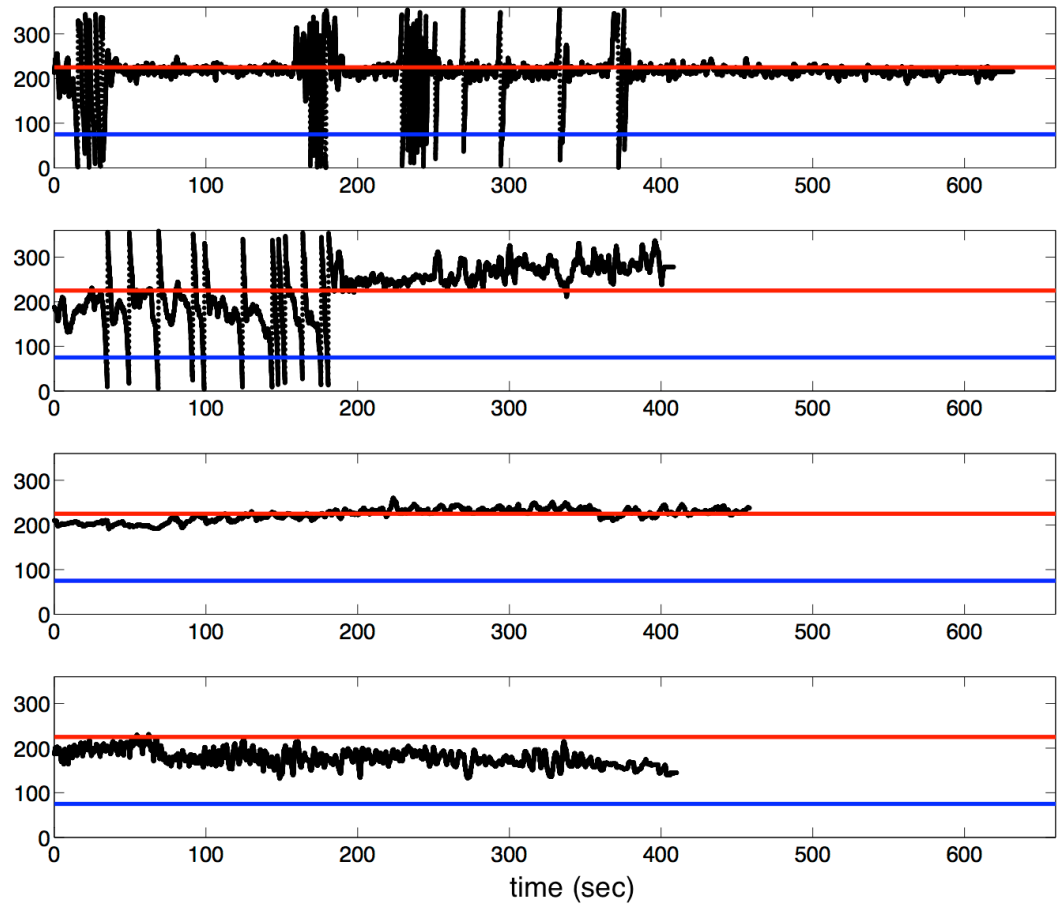

Fig. S 4. (supplement for Fig. 4) Four flight tracks in an outdoor flight simulator in the afternoon (32 minutes of flight in total) recorded in (Guerra et al. 2012), Red and blue lines correspond to the positions of the southwest and the separatrix respectively.

4. Supplementary Videos (supplement for Fig. 3 and Fig. 4)

- morning_zt_2.mp4 (Morning scenario, supplement for Fig. 3)
- midday_zt_6.mp4 (Midday scenario, supplement for Fig. 3)
- evening_zt_10.mp4 (Evening scenario, supplement for Fig. 3)
- morning_zt_2_noisy.mp4 (Morning noisy scenario, supplement for Fig. 4)

- midday_zt_6_noisy.mp4 (Midday noisy scenario, supplement for Fig. 4)
- evening_zt_10_noisy.mp4 (Evening noisy scenario, supplement for Fig. 4)